Part IV

Fe-phthalocyanine on Cr_2O_3

CHAPTER 5

Cr_2O_3 and its (0001) surface

In this chapter we study the Cr_2O_3 substrate and in particular its (001) face, considering the fundamental problem of its vacuum terminations. In particular, we compare two probable terminations through a computational approach based on DFT+U methods. From this analysis, it emerges how the two terminations can be adiabatically connected, representing two local minima in the energetic landscape, under an interval of different stresses. This underlines the relevance in terms of termination, in an experimental setup, not only of the chemical environment, but also of the mechanical stresses, i.e. of the substrates used for growth.

5.1 Bulk properties and termination problem

Cr_2O_3 has a corundum structure with space group $R\bar{3}c$ and antiferromagnetic character below the Neèl temperature of 307 K. Its AFM symmetry $\bar{3}'m'$ breaks space-inversion and time-reversal symmetries, allowing a linear magneto-electric effect [152].

We evaluate the ground state and its properties using DFT with Hubbard and VdW corrections as specified in Section 2.4. The value considered, $U_{Cr} = 4.0$ eV, was chosen following the literature so as to optimize the electronic properties (density of states) of the localized orbitals for the isolated system [12]. The first Brillouin zone is sampled through a $8 \times 8 \times 8(1)$ Monkhorst-Pack grid. The substrate is modeled with a slab that includes 6 Cr_2O_3 layers. Equilibrium geometries are obtained through a structural optimization.

From a perspective of numerical results in the bulk system, as reported in Table. 5.1, xc-PBE+U performs slightly better in terms of lattice parameter than GGA+U [12] and Hartree-Fock methods [13]. All methods underestimate the Cr spin magnetic moment, and while the former two underestimate the conduction-valence gap, the latter one overestimates it.

Table 5.1 Cr_2O_3 bulk results, for the lattice parameters, magnetic moment and conduction-valence gap, as reported in * [12] and $^\Delta$ [13].

	a [Å]	c/a	μ [μ_B/atom]	E_g [eV]
GGA+U+VdW(U=4.00 eV)	5.017	2.726	3.085	2.6
GGA*	4.941	2.798	2.68	1.2
GGA+U+J(U=5.00 eV, J=1.00 eV)*	5.073	2.727	3.01	2.6
HF$^\Delta$	5.048	2.721	3.0	$\simeq 15$
Exp.*	4.951	2.740	3.8	3.4

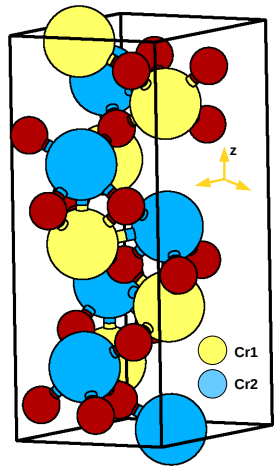

Figure 5.1 Primitive cell of Cr_2O_3 bulk. Color scheme as follows: Yellow and Blue: Cr atoms according to their respective magnetization; Red: O atoms.

The G-type antiferromagnetism is the energetically preferential magnetic configuration, other magnetic configurations are however possible at small energy differences ($\simeq 0.03$ eV) per formula unit [13]. This is the consequence of the low coupling between the Cr bi-layers along the $[001]$ direction. Another interesting feature of Cr_2O_3 is to be an intermediate Charge-Transfer-Mott-Hubbard insulator [153]. This is related to the hybridization of the correlated states in proximity of the valence-conduction gap with some delocalized states, as can be observed in the PDOS in Fig. 5.2 at the O-p mixed Cr-d valence state. The main difference with the results reported in [12], is a major spreading of the O states and Cr states in the valence band; this difference is probably related to the use of the U correction.

At this point, if we are interested in the $Cr_2O_3(0001)$ surface, instead, an understanding of the termination is needed. Different terminations have been proposed over time [9, 12]: bulk-truncated with O (a in Fig. 5.3) or Cr terminations (b and e in Fig. 5.3), enriched with O (f in Fig. 5.3) or Cr (d in Fig. 5.3) and not-enriched (c in Fig. 5.3).

The O chemical potential can favour one surface composition with respect to the other, making from the experimental point of view relevant to control temperature and O pressure conditions of the system.

In ultra-high vacuum (UHV) conditions as well as in a wide range of values of the O chemical potential, then, the Cr-terminated surface (bulk single Cr truncated), in Fig. 5.4 (a), should be the one expected. However, the experimental results [9] show the possibility of another termination in these conditions, i.e. the O-terminated one with excess of Cr atoms in the first Cr layer , in Fig. 5.4 (b).

Our experimental counterpart (POLIMI) has reached conclusions analogue to the latter ones, and through DFT+U methods, we have shown how the stress induced by a lattice mismatch between the underlying substrate and Cr_2O_3 layers is equally relevant as the O chemical potential in terms of displayed termination.

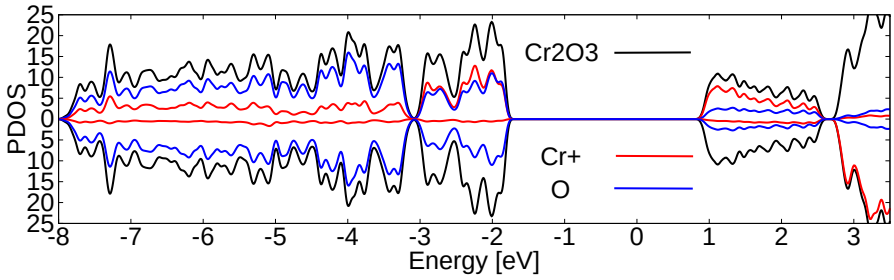

Figure 5.2 PDOS of Cr_2O_3 bulk obtained considering the GGA+U+VdW setup. Color codes: black: all unit cell atoms; red: all Cr atoms with "up" magnetic moment; blue: all O atoms. Spin-down components are shown as negative values. All values in states/eV/cell. The position of the Fermi energy in the gap is arbitrary.

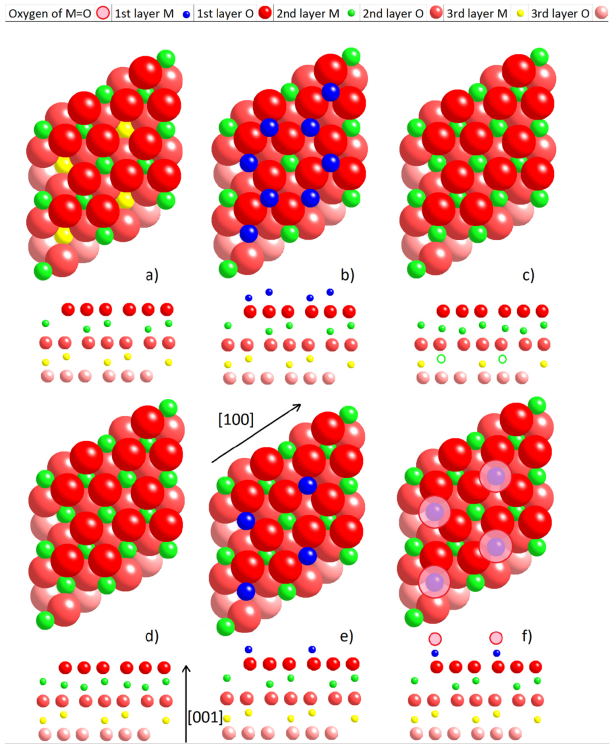

Figure 5.3 Models of Cr_2O_3(0001) surface in top- and side-view. (a) Bulk-truncated with O termination; (b) bulk-truncated with Cr termination; (c) extra interstitial metal in first layer compensated by metal vacancies in second metal layer (indicated by open circles); (d) same as (c) but without subsurface vacancies (called in the text O-terminated); (e) partial metal termination (called in the text Cr-terminated); and (f) surface with double bonded oxygen (chromyl groups). Reproduced from [9].

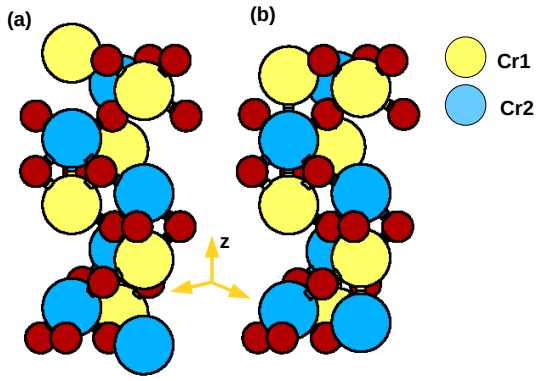

Figure 5.4 Unit cell of Cr_2O_3(0001)1x1 in its (a) Cr-terminated configuration and (b) O-terminated Cr-rich configuration. Color scheme as follows: Yellow and Blue: Cr atoms according to their respective magnetization; Red: O atoms.

5.2 Experimental evidence of O-terminations

We will show below how the O-terminated surface is a local minimum in the ground-state energy landscape, under certain conditions of stress. It means that it can be realized through the growth of Cr_2O_3 on surfaces with the proper lattice parameters or symmetries. Our experimental collaborators (POLIMI) have chosen a Cu(110) crystal as substrate on which they have studied the growth.

In the case of our experimental counterpart (POLIMI), the termination is induced by the growth of Cr_2O_3 over a Cu(110) substrate. In Fig. 5.5 the LEED patterns of the Cu(110) and of the Cr_2O_3 on Cu(110) surface for different coverages are reported.

The Cr_2O_3(0001) is incommensurate with respect to the Cu(110) underneath; in fact, while the former has hexagonal symmetry and an in-plane lattice parameter $a_{Cr_2O_3} = 4.96$ Å, the latter has rectangular symmetry and lattice parameters $a_{100} = 3.60$ and $a_{110} = 2.55$ Å. This produces a strain of the Cr_2O_3 lattice parameter. The hexagonal patterns of Cr_2O_3 appear in the LEED patterns at different coverages. The induced reciprocal lattice parameter $b_{induced}$ is then related to the one of the Cu(110), with an additional rotation

$$b_{induced} \simeq \frac{2\pi}{a_{110}} \Rightarrow \frac{2\pi}{a_{induced}\sin(\pi/3)} \simeq \frac{2\pi}{a_{110}} \Rightarrow a_{induced,FM} \simeq \frac{2}{\sqrt{3}} a_{110} = 2.95\ \mathring{A} \tag{5.1}$$

$$a_{induced,AF} = \sqrt{3} a_{induced,FM} = 5.10\ \mathring{A} \tag{5.2}$$

where a distinction between the ferromagnetic (FM) and the antiferromagentic (AF) Cr_2O_3(0001)1x1 cell has been done.

The periodicity induced on the surface Cr_2O_3 is then different from the one of the bulk Cr_2O_3. In spite of the fact that the effect could be explained as the formation of CrO, the XAS spectrum can be only associated to the Cr_2O_3. So the induced lattice parameter is then an effect of the surface reconstruction and not of a stoichiomety change. A mild strain of 2.8% with respect to the bulk lattice parameter allows a commensurate grow of Cr_2O_3 along the direction $[110]$ of the substrate, and the LEED pattern can be explained supposing the exposition of the substrate of Cr_2O_3 of its O-terminated surface.

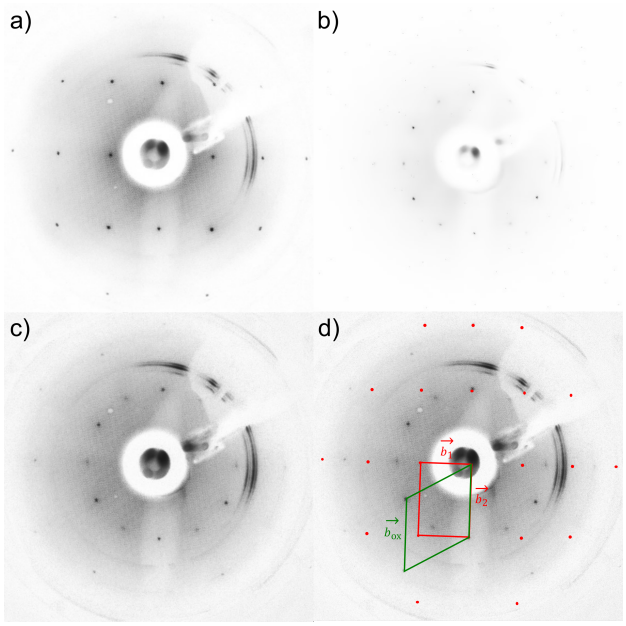

Figure 5.5 LEED patterns taken at $E = 175$ eV on: a) clean Cu(110); b) 1.2 nm-thick Cr_2O_3 on Cu(110); c) 2.5 nm-thick Cr_2O_3 on Cu(110). d) Comparison between a) and c) LEED patterns, with corresponding reciprocal unit cells, in red for Cu(110) and in green for Cr_2O_3/Cu(110). Credits: Alberto Brambilla et collaborators, POLIMI.

In Fig. 5.6 STM images of Cr_2O_3 on Cu(110) for different coverages are reported. Islands along the $[110]$ direction, flat, with an average height of about 1 nm, suggest the formation of a fully developed Cr_2O_3(001)1x1 unit cell.

5.3 Theoretical support for O-termination

To set up a structural model for the Cr-terminated Cr_2O_3 surface, we start from the 1x1 unit cell. We then move the Cr termination atoms inward of a certain length ($\simeq 0.1$ Å), we perform a structural relaxation, fixing the Cr termination atoms position along the direction normal to the surface (z in Fig. 5.4). Different strains have been applied, in order to reproduce the conditions of commensurate and incommensurate growth of Cr_2O_3(0001) on different substrates.

From these studies, reported in Fig. 5.7, it emerges that for a large window of stresses and at 0 K temperature conditions, the O-terminated surface is a local minimum in the ground-state energy landscape, i.e. it is a stable solution of the DFT problem, with respect to structural perturbations.

In particular, in Fig. 5.7, the 0 corresponds to the Cr-terminated surface, and for each step of Cr termination atoms displacement the ground-state energy of the new structure is compared to the Cr-terminated surface. When the Cr termination atom crosses the O atoms of the surface tri-layer (Cr-3O-Cr) (Fig. 5.8), the structure changes from a Cr-terminated surface to an O-terminated surface, i.e. negative values in Fig. 5.9.

However, the O-terminated surface to be physically possible, has to be stable under

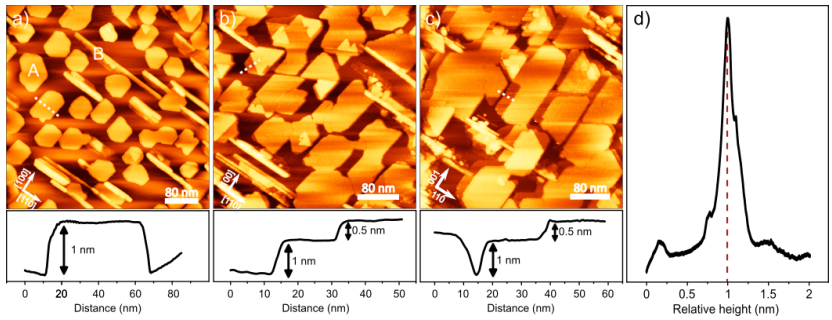

Figure 5.6 a)-c) STM images of Cr_2O_3 on Cu(110) with thicknesses 0.6 nm, 0.9 nm, and 1.2 nm, respectively. The letters A and B indicate different kind of islands (see text). All images have size $400 \times 400\,nm^2$ and setpoint ΔV = -1.8 V, I = 0.1 nA. d) Height histogram of the Cr_2O_3 islands of of panel a). Credits: Alberto Brambilla et collaborators, POLIMI.

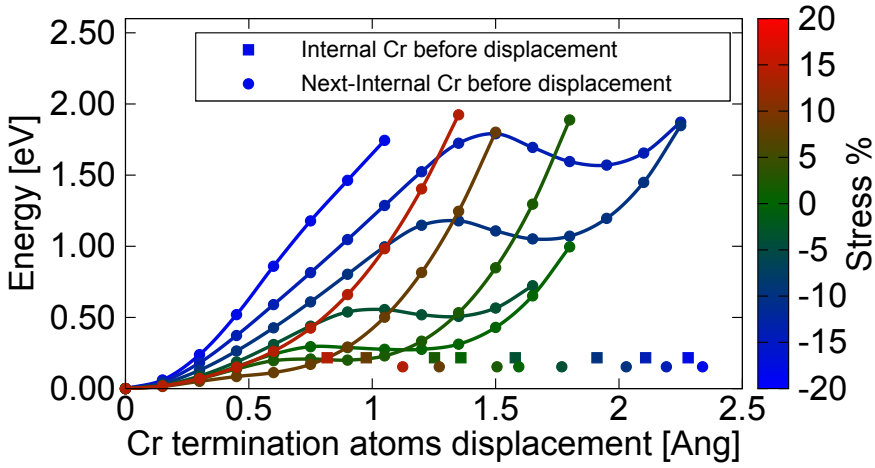

Figure 5.7 Energy (per 1x1 surface unit of 6 tri-layer thickness) versus Cr top-surface atom displacement, at different stresses. The energy is with respect to the one of the Cr-terminated surface. As square and circles, respectively, the positions of the two Cr bi-layer atoms before any displacement.

structural perturbations, in particular under structural perturbations along the direction normal to the surface (being structurally stable in the in-plane direction). This translates into the appearance of a minimum in the ground-state energy curve at varying Cr termination atoms displacement.

We notice in Fig. 5.7 as decreasing the lattice parameter (negative stress), the depth of the local minimum associated to the O-terminated surface, increases. On the other hand, when enlarging the lattice parameter (positive stress) this same local minimum disappears. In this regard, we have supposed the following explanation: the increase in energy of the local minimum with negative stress can be linked to the major available space between the O layer and the Cr bi-layer, and so to a lower interaction between the

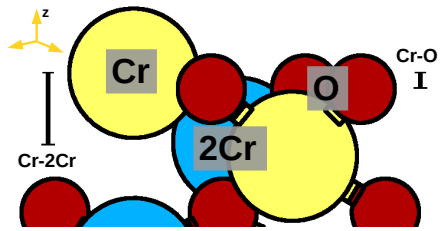

Figure 5.8 Side view of the Cr2O3(0001) in its Cr terminated surface. The distances reported in the text are here indicated. Color scheme as follows: Yellow and Blue: Cr atoms according to their respective magnetization; Red: O atoms.

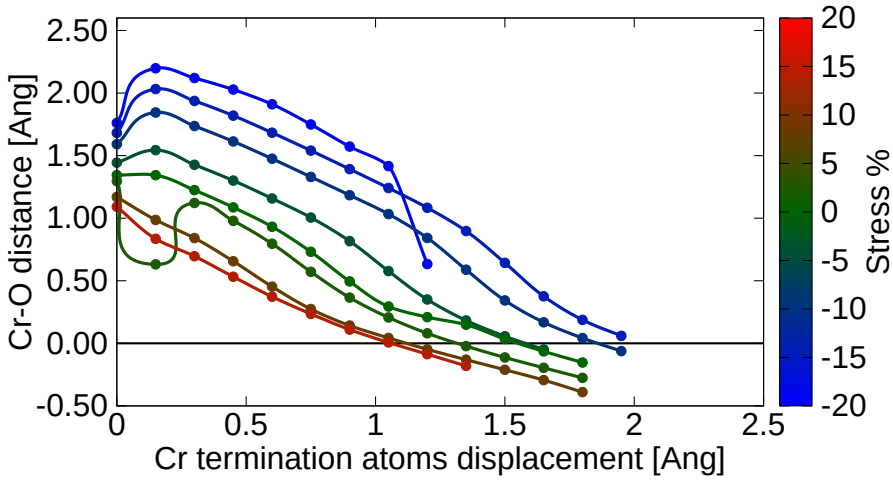

Figure 5.9 Cr-O distance versus Cr termination atoms displacement curve at different stresses. The Cr-O distance is the distance between the Cr top-surface atoms, i.e. Cr termination atoms, and the O layer of the surface tri-layer Cr-3O-Cr.

atoms, while the decrease can be linked to a decrease in the available space, and so to an higher interaction between the atoms.

In this regard, we can check as well the distance between the Cr top-surface atom and the internal Cr bi-layer in Fig. 5.10 (called Cr-2Cr in Fig. 5.8) and the thickness of the internal Cr-bilayer in Fig. 5.11. In the Cr-terminated surface, for example, for positive stresses the thickness of the internal Cr-bilayer reaches 0.30 Å, while for negative stresses it reduces to 0.05 Å. The continuity of the curves above Figs. 5.9- 5.10, except for one outlier, and their monotonic trend justify our explanation and underline a tunability of the surface termination for those stresses at which the O-terminated surface is stable.

From an experimental perspective, it is necessary not only to quantify how stress can favour the O-terminated surface with respect to the Cr-terminated surface, but also how much, in the Cr-terminated surface the stress costs. In Fig. 5.11 we report the cost in energy to change the stress considering as the minimum configuration the one with

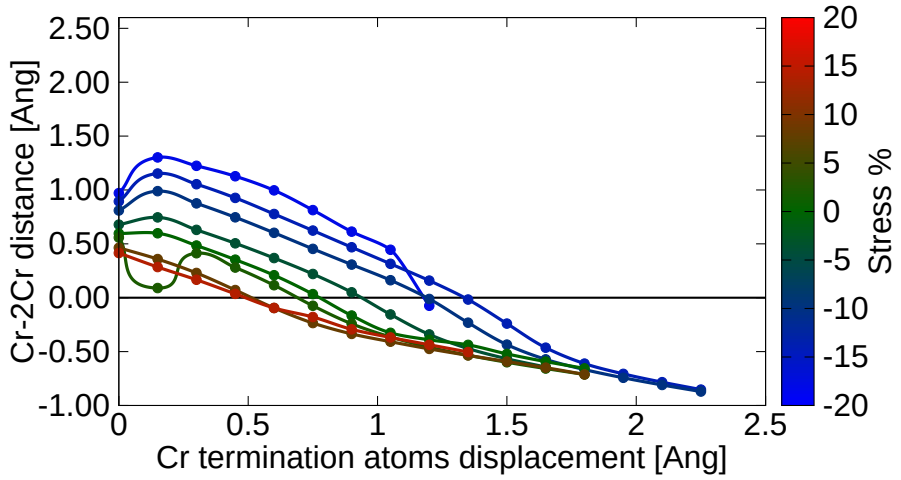

Figure 5.10 Cr-2Cr distance versus Cr termination atoms displacement curve at different stresses. The Cr-2Cr distance is the distance between the Cr top-surface atoms, i.e. Cr termination atoms, and the Cr bi-layer of the top surface tri-layers Cr-3O-2Cr-3O.

lattice parameter 5.00 Å.

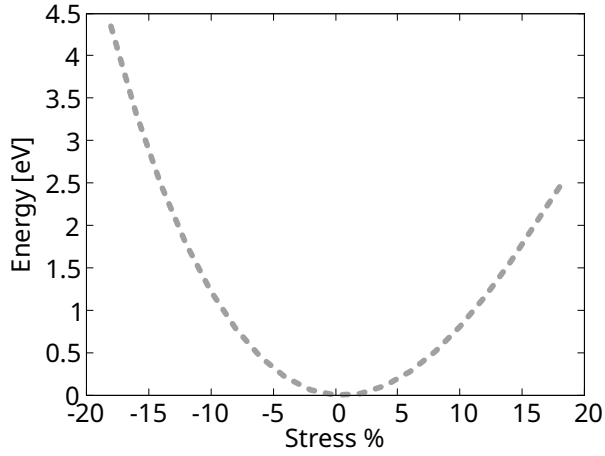

Figure 5.11 Energy difference (per 1x1 surface unit of 6 tri-layer thickness) between the stressed Cr-terminated surface and the unstressed one (the one with lattice parameter $\simeq 5$ Å) at different stresses.

The curve is slightly shifted, because the proper minimum configuration has lattice parameter 5.02 Å. We can quantify that a stress of $\simeq 10\%$ is expected to cost $\simeq 2$ eV per surface-unit., while a stress of $\simeq 2\%$ is expected to cost less than 1 eV per surface-unit (0.11 eV). At this point, reminding that for a stress of 2%, the cost in energy to obtain the

O-terminated surface from the Cr-terminated surface is less than 0.5 eV, the experimental observation of this termination surface seems quite plausible.

5.4 Magnetic configuration of the O-terminated surface

In this section, we check the magnetic stability of the obtained meta-stable state, i.e. the O-terminated surface, by mapping the DFT results onto a Heisenberg model (as described in the Section 2.3.2)

$$\hat{H} = \frac{1}{2}\sum_{ij} J_{ij}\hat{S}_i\hat{S}_j \,. \tag{5.3}$$

For this purpose we consider the surface Cr_2O_3(0001) 4x4 super-cell in its O-terminated configuration, with a 4 tri-layer thickness and a stress of 2.8% (experimental one on Cu(110), POLIMI). The coordinates of the substrate atoms are the ones of the minimum adsorption configuration in the FePc/Cr_2O_3(0001) O-terminated surface; in fact, we initially did these calculations in order to quantify the perturbation of the molecule on the exchange couplings of the substrate. However, this is not a problem, due to the fact that the substrate is not significantly perturbed in terms of the structure by the molecule in this particular spinterface. Moreover, we tested the conclusions from this mapping in a properly relaxed structure, as explained below.

In the mapping we have specifically considered only four surface atoms and flipped their spins, Fig. 5.12, while the rest of the substrate has been considered as a unique entity (bath) and left un-flipped in its ground-state configuration.

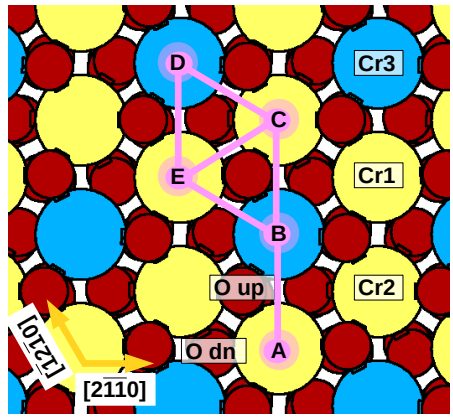

Figure 5.12 Top view of the Cr_2O_3(0001) 4x4 O-terminated super-cell. Color scheme as follows: Yellow and Blue: Cr atoms according to their respective magnetization; Red: O atoms; Magenta: selected Cr atoms in the DFT-Heisenberg mapping. The distinction between the Cr1, Cr2 and Cr3 is with respect to their height normal to the surface (Cr1 is the Cr termination atom). Analogously, the nomenclature O-up and O-down distinguishes between the O in the top tri-layer and the O in the sub-surface tri-layer.

In the Table 5.2 below, we report the obtained exchange couplings between the selected atoms and the rest.

Table 5.2 Exchange couplings (meV) obtained from the mapping of the DFT calculations and the Heisenberg model in Eq. 5.3. The atoms considered in the Heisenberg model are the one in magenta in Fig. 5.12, while the other atoms of the substrate have been considered as a bath.

	A↑	**B↓**	**C↑**	**D↓**	**E↑**	**Rest**
A↑	0.00	-10.81	-1.83	-0.83	-4.58	183.27
B↓	-10.81	0.00	-0.15	-0.68	-23.66	-37.29
C↑	-1.83	-0.15	0.00	-9.61	-13.41	-5.55
D↓	-0.83	-0.68	-9.61	0.00	-21.02	-172.61
E↑	-4.58	-21.66	-13.41	-21.02	0.00	-15.20
Rest	183.27	-37.29	-5.55	-172.61	-15.20	0.00

Looking at the Heisenberg model it is clear that a parallel spin configuration is unstable if the exchange coupling is positive, while a anti-parallel one is unstable if the exchange coupling is negative. In particular, from the Table 5.2, it is clear from the negative values the preference of the atoms (A, B), (B,E), (C,D) and (D,E) to be parallel. Looking at the Fig. 5.12 the Cr1-Cr2-Cr3 instead of the up-down-up spin configuration would prefer an up-up-up spin configuration, suggesting a configuration where all surface Cr have the same spin sign.

To verify this conclusion and its stability with respect to stress conditions, we calculate again the energy curve between the Cr-terminated surface and the O-terminated surface in a range of stresses between 0% and 4%, considering a ferromagnetic top-layer instead of an anti-ferromagnetic one.

Looking at Fig. 5.13, while as expected this magnetic configuration is unstable in the Cr-terminated surface, it results the most stable one in the O-terminated surface. Thus, the meta-stable state of the Cr_2O_3 substrate, i.e. the O-terminated surface state, has the exotic feature of being anti-ferromagnetic inside and ferromagnetic outside. The difference in magnetization is due to the proximity of the Cr atoms at the top of the surface, and to the absence of O atoms favouring a super-exchange anti-ferromagnetic coupling.

5.5 Conclusions

From the computational results, the O-terminated surface appears to be a stable configuration of the substrate for a certain range of stresses. A mapping of our DFT results into an Heisenberg model, has moreover underlined the preference of the O-terminated substrate to acquire a ferromagentic ordering at the surface, preserving an antiferromagnetic one inside.

In the following chapters, we will study the adsorption of the FePc molecule on these two terminations: underlining the characteristics of the two different spinterfaces.

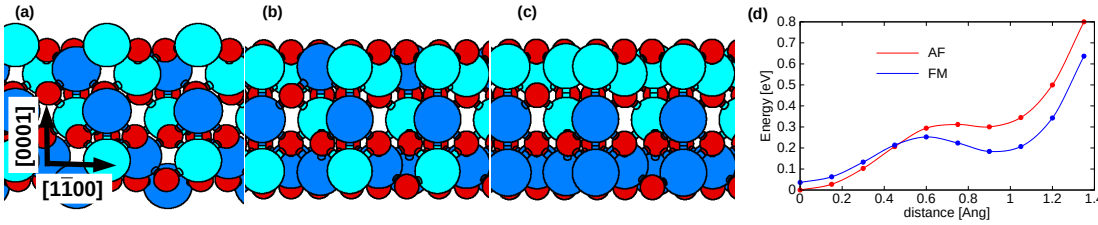

Figure 5.13 Side-view of the: (a) Cr-terminated surface; (b) Cr-rich O-terminated surface with AF ordering; (c) Cr-rich O-terminated surface with FM ordering. Color scheme as follows: light and dark blue represent spin-up and spin-down Cr atoms; red represents O. (d) Energy spent in pushing inwards the Cr atoms of the Cr-terminated surface seen in panel (a), differentiating between the two possible magnetic orderings of the outer layers, obtaining the two local minima depicted in panels (b) and (c) (per formula unit). Color scheme as follows: Light and Dark Blue: Cr atoms according to their respective magnetization; Red: O atoms.

CHAPTER 6

Fe-phthalocyanine on Cr2O3(0001), Cr-terminated

In this chapter, we study the FePc/Cr2O3(0001) assuming the Cr-terminated surface discussed previously, from an energetic, magnetic and optical point of view. A particularly interesting result is that the molecule binds through its imide N atoms to the surface, via a bidentate configuration, while the Fe atom acquires a ferromagnetic ordering with respect to the top Cr atom, due to its proximity. Regardless of the adsorption configuration, the molecule itself breaks the spin symmetry of the substrate, favouring in the optical excitation a splitting of the two spin-channels, which could suggest a coupling between the light excitation and any magnetic excitation. In this regard, the significant hybridization between the molecule and the substrate, underlines as the optical onset is lower than in the pristine systems, and how the spinterface light excitation corresponds to a movement of electronic charge from the substrate toward the molecule with influence on magnetic properties. Note that the majority of the results have already been published as [94].

6.1 Computational details

We evaluate the ground state of the FePc/Cr_2O_3(0001) spinterface and its properties using DFT in a plane-wave basis set, with U and VdW corrections, as already pointed out in the Section 2.4. This appraoch introduces some level of arbitrariness about the choice of the additional Hubbard U parameter, which inevitably influences the results. However, in this specific case, the adsorption energy is primarily dominated by the formation of bonds between the imide N atoms and surface Cr1 (yellow atoms in Fig. 6.1), with a large energy difference with respect to the other cases. So, we are confident this result is robust with respect to the choice of U. The values considered, $U_{Cr} = 4.0$ eV and $U_{Fe} = 5.0$ eV, were chosen following the literature so as to optimize the electronic properties (density of states) of the localized orbitals for the isolated systems [12, 119]; with these values, the Cr_2O_3 characteristic, intermediate between a charge transfer insulator and a Mott-Hubbard insulator, is well reproduced, as well as the magnetism of the Fe atom of the molecule. The substrate is modeled with a slab that includes 4 Cr_2O_3 layers. Equilibrium geometries are obtained through a structural optimization of the molecule and of the top three layers of the substrate. In the same way, the optical spectra are obtained and analyzed following what already pointed out in Section 2.4.

6.2 Adsorption configurations

Considering the Cr-terminated surface of Cr_2O_3(0001), we study the adsorption of Fe-phthalocynanine. We construct a 4x4 supercell which is sufficiently large to fit the molecule,

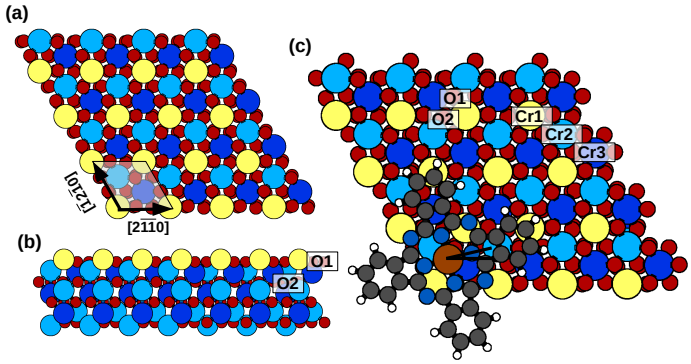

Figure 6.1 (**a**) Top view and (**b**) side view of the 4×4 surface supercell used for the calculations, with primitive cell of $Cr_2O_3(0001)$ indicated in (**a**) (shaded). (**c**) Model of $FePc/Cr_2O_3(0001)$, indicating the angle between the N-Fe-N axis and the surface $[2\bar{1}\bar{1}0]$ direction (Black lines centered on Fe atom). Color scheme as follows: yellow: topmost Cr atoms (named Cr1); light and dark blue: Cr atoms of the subsurface trilayer, according to their respective height (light higher Cr2, dark lower Cr3) in the bilayer 3O-2Cr-3O; red: O atoms. The magnetization of the Cr3 is parallel to that of the Cr1 atoms and opposite to that of the Cr2 atoms. Three of the O atoms are in the surface trilayer (O-up) and three in the subsurface trilayer (O-dn). Brown: Fe.

thereby avoiding molecule-molecule interaction. In fact, the distance between the Fe centers of 20.42 Å (the one between the H atoms is of 5.48 Å) is significantly larger than the one of 14.28 Å for packed molecules on Al(001) [154]. In Fig. 6.1 the super-cell and the molecule in its planar configuration are shown.

Different adsorption configurations of planar molecules have been considered (see Figure 6.2), which are distinguished by their adsorption site, the azimuthal angle between one of the molecule axes and the substrate $[2\bar{1}\bar{1}0]$ direction, and the magnetic configuration, i.e., with the Fe spin being either ferromagnetic (FM) or antiferromagnetic (AF) with respect to the spin of the underlying Cr1 atom (see Fig. 6.1). Concerning the adsorption sites, we start the geometry optimizations with the Fe atom placed above all the surface atoms that are visible from the top: a topmost Cr atom (Cr1), the two Cr atoms below the O_3 layer (Cr2 and Cr3, from top to bottom), an O atom of the first layer (O1) or of the second one (O2), and the bridge site between two Cr1 atoms (B).

The adsorption energies are reported in Table 8.1.

Lower adsorption energies, i.e. more negative ones, are related to the bonding between the imide N atoms and the top-surface Cr atoms, and not to the proper site of adsorption, i.e. the position of the Fe atom. The O configurations, in fact, have an higher adsorption energy (by $\simeq 0.6 - 0.7$ eV) than the Cr configurations, at those molecular angles (O-up $45°$ and O-dn $0°$) which favor this bonding (N-Cr1$\simeq 2.7$ Å). The role played by the phenyl rings is less significant, as underlined by the Cr1 configurations at $22°$ and $0°$ with a smaller increase ($\simeq 0.4$ eV). Related to this finding is the fact that the Cr3 configurations at $45°$ and $22°$ relaxed in the bridge configuration (B) at $15°$, and the fact that the rotation of the molecular axis in the bridge configuration by $75°$ to $15°$ gives a gain of 0.7 eV. In the bridge configuration at $15°$ the imide N and Cr1 bonding length is 2.47 Å.

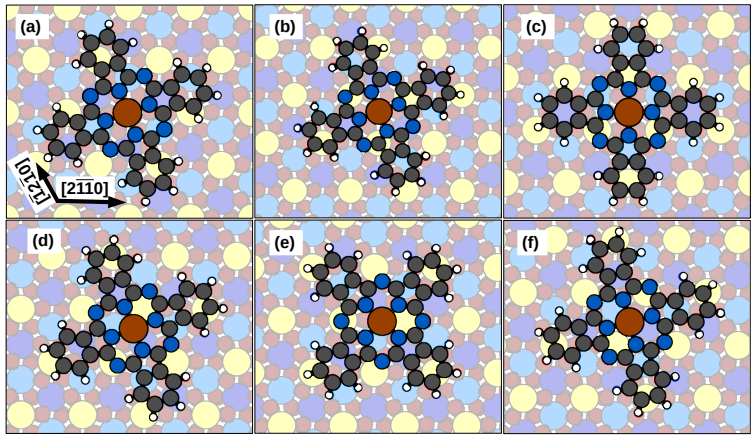

Figure 6.2 Optimized geometry for FePc/Cr_2O_3(0001) for the adsorption configurations considered: (**a**) on a Cr1 site at 22°, (**b**) on a Cr2 site at 22°, (**c**) on a Cr3 site at 0°, (**d**) on an O-up site at 22°, (**e**) on an O-dn site at 45°, and (**f**) on a B site at 15°. The color scheme is the same as in Figure 6.1.

Table 6.1 Adsorption energy for FePc/Cr_2O_3(0001) as a function of adsorption site and optimized azimuthal angle for FM and AF orientation of the Fe spin with respect to underlying Cr1 atoms. Values in eV.

Site	Angle	E_{ads}^{FM}	E_{ads}^{AF}	$E_{ads}^{AF} - E_{ads}^{FM}$ [eV]
Cr1 (up)	0°	−3.793	−3.710	0.082
	22°	−3.453	−3.860	−0.407
Cr2 (up)	0°	−3.436	−3.519	−0.083
	22°	−3.533	−3.541	−0.009
Cr3 (down)	0°	−3.493	−3.438	0.055
O-up	0°	−4.100	−4.165	−0.065
	22°	−4.202	−4.203	−0.001
	45°	−3.558	−3.575	−0.017
O-dn	0°	−3.444	−3.454	−0.010
	45°	−4.233	−4.234	0.000
B	15°	−4.316	−4.252	0.065
	24°	−4.169	−4.234	−0.065
	45°	−3.444	−3.460	−0.016
	52°	−3.494	−3.511	−0.016
	75°	−3.410	−3.394	0.016

While the adsorption energy is primarily governed by the bonding between the imide N atoms and the surface Cr atoms, the magnetic behaviour of the molecule depends on the proximity between the Fe atom and the surface Cr atoms. As can be observed in Table 6.1, when the Fe atom is near by the Cr atoms the coupling is mainly ferromagnetic, while not near the Cr atoms, an antiferromagnetic coupling is favoured, due to some super-exchange mechanism through the O atoms. This behaviour is clearly underlined

by the B configuration, where at the minimum adsorption energy angle $15°$, the Fe atom shifts partially towards the O-dn site and approaches the Cr1 atom (2.62 Å), going from an antiferromagnetic to a ferromagnetic coupling. The shift is energetically favoured, as a shift toward the O-up site would cost 0.28 eV.

6.3 Electronic properties

In this section we focus on the electronic properties for the minimum adsorption energy configuration, B $15°$ FM, by looking at the projected density of states PDOS Fig. 6.3.

Aligning the deep states which are unmodified by the adsorption of the molecule before and after the adsorption, we can observe how the molecular LUMO inside the valence-conduction gap of the clean substrate lowers in energy after the adsorption in both spin-channels (with breaking of a degeneracy in the spin-up channel). Despite the molecular HOMO lowers in energy as well, the valence-conduction gap of the adsorbed system reduces: in the spin-up channel from 1.67 to 1.07 eV and in the spin-down channel from 1.66 to 1.09 eV.

Referring to unoccupied Kohn-Sham states as "lu+n" and to occupied ones as "ho-n" (where lu and ho reduce, in the molecular system, to LUMO and HOMO, respectively), looking at Fig. 6.3 we notice as in the spin-up channel the ho, lu and lu+1 (0.2 eV above lu) (50% and 80% respectively), and in the spin-down channel the lu and lu+1 (0.38 eV above lu) ($\simeq 94\%$) have all molecular character, while the other states in proximity of the band gap, have substrate character ($> 90\%$). Away from the band gap, the orbitals with molecular character are: in the spin-up channel, at -0.52 eV below the ho (15%) and at $+1.56$ eV above the lu (50% of which 26% of Fe nature), in the spin-down channel at -0.48 eV below the ho (65% of which 40% of Fe nature) and at $+1.47$ eV above the lu (66%). Of the molecular orbitals mentioned, the ones in proximity of the band gap are mainly of C nature, and in part of N nature, whereas only those further away from the Fermi energy have Fe contributions.

Overall the PDOS of the molecule and of the substrate are not significantly affected by the adsorption. Exceptions are visible at energies below the ho of the N and C orbitals, these are the contributions from those atoms bonding with the surface Cr atoms. In the inset of the Fig. 6.3, the DOS of the bonding imide N atoms and the Cr atoms is reported. A real-space charge density difference analysis (Fig 6.4) can be used to underline these major variations, which effectively are located at the bonding points. Here, we notice that the real-space charge density difference is obtained as

$$\Delta\rho(\boldsymbol{r}) = \rho_{\text{molecule+substrate}}(\boldsymbol{r}) - (\rho_{\text{molecule}}(\boldsymbol{r}) + \rho_{\text{substrate}}(\boldsymbol{r})) \tag{6.1}$$

where $\rho(\boldsymbol{r}) = \sum_{nk\sigma} |\psi_{nk\sigma}(\boldsymbol{r})|^2$ and respectively the density of the adsorbed system (molecule+substrate) and the ones of the isolated systems (molecule and substrate) are considered.

6.4 Magnetic properties

The magnetic and electronic charge modifications due to the adsorption are reported in Fig. 6.5. These modifications are computed as the differences in the Lowdin populations between the full spinterface and the free standing molecule (panels (b) and (e)) or the uncovered substrate (panels (a),(c),(d) and (f)).

The variations are mainly localized at the top of the substrate, with small contributions from the subsurface layers. This underlines how the interaction between the

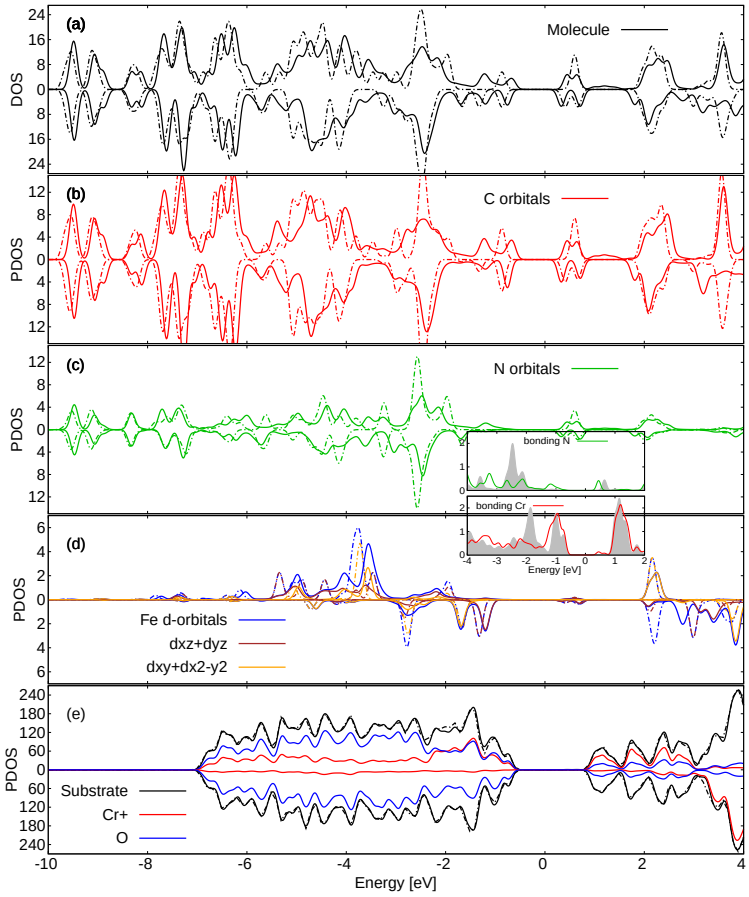

Figure 6.3 Electronic PDOS of $FePc/Cr_2O_3(0001)$ summed over (**a**) all molecule atoms; (**b**) C; (**c**) N; (**d**) Fe; (**e**) substrate atoms. Substrate color codes: black: all substrate atoms; red: all Cr atoms with "up" magnetic moment; blue: all O atoms. Solid/dash-dotted lines indicate adsorbed and gas phase molecules, respectively. Spin-down components are shown as negative values. All values in states/eV/cell. The position of the Fermi energy in the gap is arbitrary. In the inset, we report the spin-up contributions from the bonding imide N and Cr1 (lines) atoms over the other imide N and Cr1 atoms (gray area).

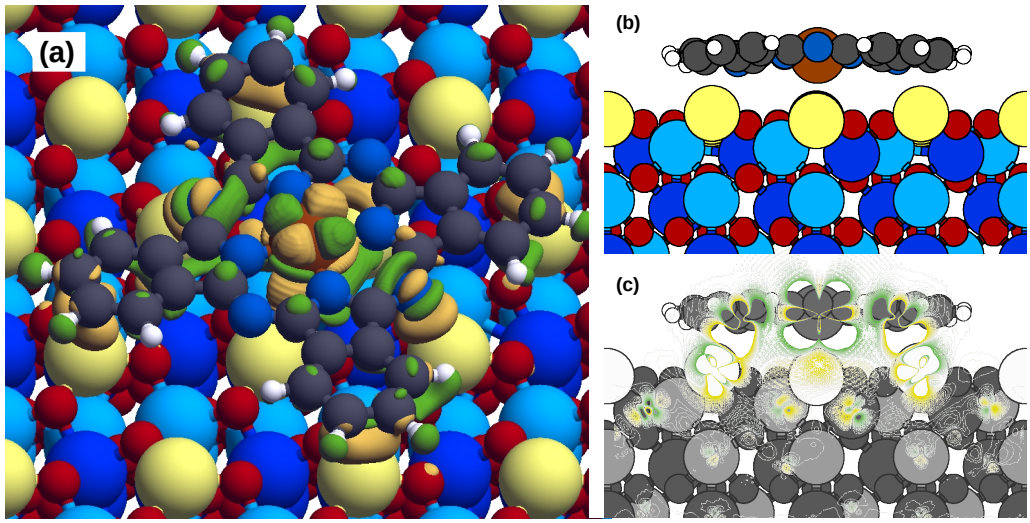

Figure 6.4 On the left, (**a**) top view; on the right, (**b**,**c**) side-view of the charge density difference in the FePc/Cr_2O_3(0001) minimum energy adsorption configuration (isovalues in the range of 0.001 Å $\times$ 10^{-3}). Note the major variations between the imide N and the Cr1 and between the phenyl rings and the Cr1. Color scheme the same as in Figure 6.1.

molecule and the substrate is mainly localized at the interface. The bonding Cr1 are the most affected ones, and the ones bonding to the imide N atoms ($\Delta\mu \simeq -60 \times 10^{-3}\mu_B$) and the ones under the phenyl rings ($\Delta\mu \simeq -20/60 \times 10^{-3}\mu_B$). To these magnetic variations correspond analogue electronic charge variations, as the bonding Cr atoms show a depletion of electronic charge ($\simeq 38 \times 10^{-3}\ e^-$), while the molecule acquires electronic charge at the N imide atoms ($\simeq 40 \times 10^{-3}\ e^-$). The molecule acquires overall 0.19 electrons, that are not evenly distributed: the external imide N atoms and the C atoms acquire respectively 0.105 and 0.143 electrons, while the inetranl pyrrolic N atoms and the H atoms lose respectively 0.053 and 0.049 electrons. The Fe magnetic moment (free molecule $2.17\mu_B$) is not significantly affected by the adsorption, in spite of the electronic charge variations; probably, these involve mainly the s orbital.

6.5 Optical properties

Now we discuss the optical properties of FePc/Cr_2O_3(0001) in the minimum adsorption configuration, reporting the $2D$ polarizability in Fig. 6.6, for the adsorbed system and for the pristine one (the optical spectrum of the isolated molecule has been already described in Section 3.6). The intensities of the three spectra are scaled by the same factor, chosen so to normalize the transition at $\simeq 1.5$ eV in the free molecule to unity. An average of the in-plane directions has been considered.

The adsorption of the molecule reduces the optical gap of the substrate, due to the energetically low optical transitions of the free molecule. The modifications in the spinterface peaks corresponding to the free molecule ones underline a significant hybridization at the interface, as already notice in the PDOS (Fig. 6.3). In the lower inset of Fig. 6.6, the relative intensities of the transitions are reported in red, for the two spin-channels, nor-

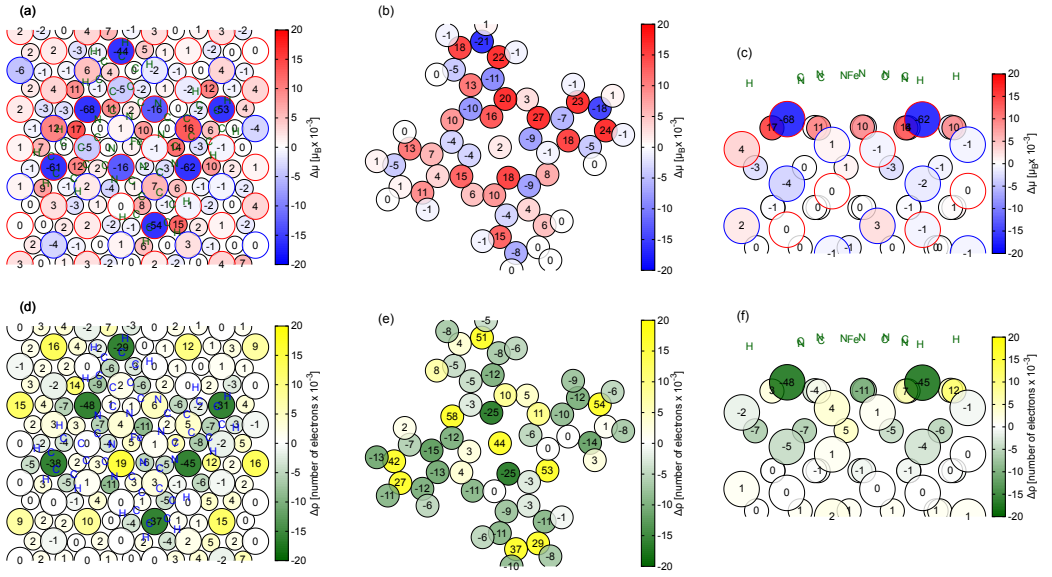

Figure 6.5 Variations in the atomic magnetic moments of FePc/Cr_2O_3(0001), seen from the top, with respect to the isolated systems, on (**a**) the surface and on the molecule (**b**). Corresponding variations in the electronic density (**d**,**e**). (Positive = increase in electron population.) Side view of the variations: (**c**) magnetic moments and (**f**) charge density. The positions of the molecule atoms are marked by green/blue letters in panels (**a**,**c**,**d**,**f**). Notice that few values in the plot exceed the maximum ones on the scale bar.

malized with respect to the maximal one at $\simeq 1.1$ eV (bins with relative intensity lower than 10% of the maximal one are omitted). In the upper inset of Fig. 6.6, the molecular contributions (yellow) to the valence and conduction states $P_b^{(v/c)}$ are reported for each transition (purple).

The first part of the spinterface spectrum (< 1.50 eV) (red curve in Fig. 6.6) resembles the energy-shifted free molecule one, considering the additional breaking of the partial degeneracy in the spin-up channel (the two degenerate peaks at $1.46 - 1.47$ eV split into the two separated peaks at 1.09 eV and 1.24 eV), which is induced by the interaction with the spin-up polarized Cr1 atoms. On the other hand, while the conduction states of these transitions preserve the molecular nature (80%), the valence states have, instead, major contributions from the substrate ($40-70\%$). This implies that upon light excitation, electron density moves from the substrate toward the molecule. In particular, due to the fact that the adsorption of the molecule breaks the spin-symmetry of the substrate, we expect this movement of charge would be characterized by a majority of a certain spin channel electrons.

Taking the height of the Cr1 atoms as a reference $z = 0$ (so that the Fe atom is at $z_{Fe} = 2.60$ Å) (Table 6.2) and considering the two main peaks in the spin up channel, the weighted height of the valence levels amounts to $z^{(v)} = -0.8 \pm 0.1$ Å, between the Cr1 and the top bilayer atoms Cr2-Cr3, while the one of the conduction levels amounts to $z^{(c)} = 1.5$ Å (1.2 Å below the molecule) (as reported in Table 6.3). Considering instead the two main peaks in the spin down channel, $z^{(v)} = 0.1$ Å and $z^{(v)} = -1.5$ Å, close